Journal of the Serbian Chemical Society
JSCS-info@shd.org.rs • www.shd.org.rs/JSCS

ACCEPTED MANUSCRIPT

Journal of the Serbian Chemical Society
JSCS-info@shd.org.rs • www.shd.org.rs/JSCS
J. Serb. Chem. Soc. **00(0)** 1-16 (2026)
JSCS–13599
Original scientific paper
Published DD MM, 2026

Efficient one-pot solvothermal synthesis of lanthanum-iron oxide and its application in tenofovir adsorption

ZHIGANG LIU[1], PING XU[2], SHIHUA YU[2], XIANG LI[1], XIAODAN ZENG[3], JIBO ZHANG[1]*, AND JUNJING HAO[4]

[1]*College of Petrochemical Technology, Jilin University of Chemical Technology, Jilin 132022, China,* [2]*College of Chemical & Pharmaceutical Engineering, Jilin University of Chemical Technology, Jilin 132022, China,* [3]*Centre of Analysis and Measurement, Jilin Institute of Chemical Technology, Jilin 132022, China, and* [4]*China Petroleum Jilin Chemical Engineering Co., Ltd., Jilin 132000, China.*

(Received 25 October 2025; revised 26 January 2026; accepted 1 July 2026)

Abstract: A novel magnetic lanthanum-iron oxide composites have been synthesized using a one-pot method. The proposed approach simplifies the synthesis process by eliminating traditional requirements such as pH adjustment and high-temperature calcination, resulting in a more streamlined procedure and production of a magnetic material. The effects of the Fe-to-La ratio, reaction time, and reaction temperature on the properties and adsorption performance of the lanthanum-iron oxide composites were investigated. The synthesized composites were characterized by SEM, XRD, VSM, FTIR, BET, TGA, and XPS, which indicated that the samples comprised of randomly oriented particles with sizes ranging from 20 to 200 nm, it possessed excellent crystallinity, magnetic responsiveness and thermal stability. Additionally, this study also explored the application of lanthanum-iron oxide in adsorbing tenofovir ((*R*)-9-(2-phosphonomethoxypropyl)adenine, PMPA), with the maximum adsorption capacity of 34.06 mg/g, under the conditions of adsorbent dosage=0.9 g/L, pH=4, *C*=50 mg/L, and *T*=25 °C. The prepared lanthanum-iron oxide was simple to prepare and enabled rapid separation, which was beneficial to practical applications.

Keywords: one-pot synthesis; lanthanum-iron oxide; superparamagnetism; adsorption; pharmaceutical intermediates.

INTRODUCTION

As a notable transition metal oxide, lanthanum-iron oxide predominantly comprises variations including $LaFeO_3$,[1] $La_{1-x}Sr_xFeO_{3-\delta}$,[2] and Fe/La_2O_3,[3] exhibiting diverse compositions and valencies. Its widespread research interest stems from its

* Corresponding author. E-mail: 763976113@qq.com
https://doi.org/10.2298/JSC251025034L

abundant availability, non-toxic nature, and exceptional chemical stability.[4] Lanthanum-iron oxide has been employed in various applications, such as electrodes,[5] chemical sensors,[6] adsorbents,[7] and catalysts.[8-9] The performance of magnetic composites is influenced by its stoichiometric composition and microstructure, shaped during the synthesis process. Therefore, the choice of synthesis method varies, depending on its intended application. Established synthesis techniques include high-energy milling,[10] citrate-gel method,[1] co-precipitation,[11] hydrothermal method,[12-13] and microwave-assisted method.[14] The first three methods yield magnetic lanthanum-iron oxide compounds with particle sizes ranging from 10 to 50 nm, requiring high-temperature calcination for enhanced crystallinity.[15] The citrate-gel and co-precipitation methods additionally necessitate pH adjustment. While microwave-assisted synthesis avoids calcination and pH adjustment,[14] it produces gases during combustion, resulting in samples with weaker magnetic properties.

In a pharmaceutical context, (*R*)-9-(2-phosphonomethoxypropyl)adenine (PMPA), also known as tenofovir, is a key intermediate in immunodeficiency therapy that contains a phosphate group.[16] However, the pharmaceutical wastewater generated during the production of PMPA contains about 1–2% of the product, which is considered harmful pharmaceutical pollutants in the environment. Therefore, it is of great importance to remove PMPA in wastewater from the syntheses of pharmaceutical intermediates. In recent years, there are few reports on the removal of tenofovir, and the treatment methods for pharmaceutical wastewater can generally be divided into two categories: quantitative recovery and degradation elimination.[17] Among them, quantitative based remove can alleviate the pressure of downstream wastewater treatment, which has attracted increasing attention from researchers. The commonly used methods for quantitative separation in industry include multi effect evaporation,[18] membrane separation,[19] adsorption,[20-21] and recrystallization.[22] Among them, adsorption has become an attractive approach owing to its economic cost, high efficiency and easy operation.[23] Extensive investigations have revealed that metal (hydr)oxides have strong affinity for phosphate due to the formation of inner-sphere complexes between phosphate species and the functional groups of the adsorbents.[24-25] So far, lanthanum (La)-based materials are attended widely for phosphate removal even at low concentrations due to the strong affinity of La towards phosphate and the low solubility product of $LaPO_4$ (pKsp=26.15).[23, 26] Xiong et al. prepared La-doping Mn-Al bimetal oxide composites for phosphate adsorption with the equilibrium state at pH=7 after 5 h.[27] Qiu et al. fabricated a new composite Ws-N-La by anchoring nano-La(III) (hydr)oxides within a quaternary-aminated wheat straw for phosphate adsorption, the maximum adsorption capacity increased from 19.6 to 67.1 mg P/g.[28] However, due to tedious separation problem caused by highly dispersed materials, magnetization has received widespread attention as an

environmentally friendly approach, which can not only enhance the recovery performance of materials, but also improve their adsorption capacity.

Currently, only Ajebli et al.,[29] have conducted studies on the removing of tenofovir, they utilized activated carbon prepared through phosphoric acid thermochemical activation for PMPA adsorption. This process involved multiple steps including washing, drying, and thermal activation of corn cobs, followed by pH adjustment and drying of the resulting porous carbon. In contrast, we have developed a novel one-pot synthesis method to prepare lanthanum-iron oxide compounds, effectively avoiding the need for pH adjustment and high-temperature calcination, thus significantly streamlining the synthesis process. The resulting magnetic composite offers a rapid separation of PMPA from pharmaceutical wastewater under an external magnetic field, demonstrating a more efficient and potentially impact approach for pharmaceutical waste management.

In summary, we have dedicated to prepare lanthanum-iron oxide by a straightforward and efficient one-pot synthesis method. This novel approach not only simplifies the preparation process but also shows potential in adsorption of PMPA from pharmaceutical wastewater. The performance of lanthanum-iron oxide was assessed using batch experiments, demonstrating its ease of preparation, fast separation, and exceptional adsorption properties.

EXPERIMENTAL

Materials

Analytical grade reagents were procured for the experiments. Sodium acetate trihydrate ($CH_3COONa·3H_2O$) and ferric chloride hexahydrate ($FeCl_3·6H_2O$) were sourced from Shanghai McLean Biochemical Technology Co., Ltd., while lanthanum nitrate hexahydrate ($La(NO_3)_3·6H_2O$) and ethylene glycol (EG) were purchased from Sinopharm Chemical Reagent Co., Ltd. Tenofovir (PMPA, $C_9H_{14}N_5O_4P$) was obtained from Jilin Sihuan Pharmaceutical Co., Ltd. The chemical structure of tenofovir is illustrated in Fig. 1.

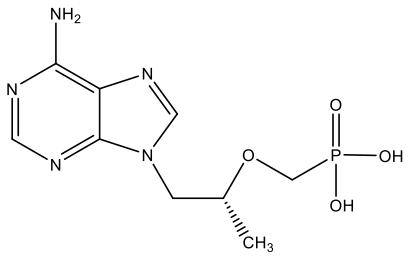

Fig.1. Chemical structure of tenofovir.

Characterization of the lanthanum-iron oxide compounds

Tenofovir concentrations were determined via UV-visible spectroscopy (UV-2550, Shimadzu, Japan). The surface morphology and crystal structure of composites were obtained by scanning electron microscopy (SEM, Regulus-8100, Hitachi, USA) and X-ray diffraction (XRD, D8FOCUS, Bruker, Germany). The magnetic property of the sorbents was analyzed with

a vibrating sample magnetometry (VSM, 7404, Lake Shore, USA). Fourier-transform infrared (FTIR) spectroscopy (NICOLET6700, Thermo Fisher, USA) for functional groups, Brunauer-emmett-teller analysis (BET, JW-BK200B, JingWeiGaoBo, China) for specific surface area, and X-ray photoelectron spectroscopy (XPS, AXIS, Shimadzu, Japan) for elemental chemical states of samples. The thermal stability of the nanocomposites was analyzed on a blast drying oven (DHG-9070A, Yiheng Technology Co., Ltd., China), a thermogravimetric analysis and differential scanning calorimetry (TGA-DSC) high-temperature synchronous thermal analyzer (Discovery SDT650, Swart, USA).

Preparation of lanthanum-iron oxide compounds

The synthesis process involved heating 60 mL of EG to 70 °C, followed by adding $FeCl_3 \cdot 6H_2O$ and $La(NO_3)_3 \cdot 6H_2O$ in varying amounts to achieve Fe-to-La molar ratios of 0:1, 1:0, 6:1, 8:1, and 10:1. After magnetic stirring until dissolution, 7.2 g of sodium acetate trihydrate was added and stirred for 10 min. The effect of temperature and reaction time on lanthanum-iron oxide preparation were examined by reacting at 200, 210 °C for 6, 8, 10, 12 h in a hydrothermal reactor. Post reaction, the product was cooled, washed, and dried at 70 °C to obtain brown lanthanum-iron oxide powders. Optimize preparation conditions (such as molar ratios, temperature and time) were obtained based on the performance of lanthanum-iron oxide for PMPA removing.

Adsorption experiments

Adsorption of PMPA. The adsorption properties of lanthanum-iron oxide for PMPA were extensively investigated under various conditions. The experiments assessed the impact of lanthanum-iron oxide dosage, temperature, and pH on PMPA adsorption. For the dosage study, varying amounts of lanthanum-iron oxide (5 to 40 mg) were added to a three-necked flask containing 40 mL of 50 mg/L PMPA solution at 25 °C, with stirring at 520 rpm. Upon reaching adsorption equilibrium, samples were filtered through a 0.22 μm organic membrane for UV spectrophotometric analysis of the remaining PMPA concentration. The effect of temperature on PMPA adsorption was examined by adding 35 mg of lanthanum-iron oxide to 40 mL of 50 mg/L PMPA solution at 25, 35, and 45 °C. Additionally, the influence of pH was explored by adjusting the pH of a similar PMPA solution to values ranging from 3 to 8 using 0.1 M hydrochloric acid or sodium hydroxide, followed by the addition of 35 mg of lanthanum-iron oxide. The adsorption capacity (q_e) and removal efficiency (R%) were calculated using Eqs. (Eq1, Eq2).

$$q_e = \frac{(C_0 - C_e)}{m} \times V \quad (1)$$

$$R = \frac{C_0 - C_e}{C_0} \times 100\% \quad (2)$$

C_0 and C_e are the initial and equilibrium concentrations of PMPA (mg/L), m is the mass of the material (mg) and V is the solution volume (L).

Adsorption kinetics. A kinetic study involved dispersing 35 mg of lanthanum-iron oxide in 40 mL of a 50 mg/L PMPA solution at room temperature (RT, 20 °C). Samples were collected at set intervals to determine the residual PMPA with UV spectrophotometric measurement.

Adsorption isotherm. Subsequently, an adsorption isotherm experiment was conducted at RT. Here, 35 mg of lanthanum-iron oxide was added to 40 mL of PMPA solution with concentrations ranging from 30 to 80 mg/L to ascertain the maximum adsorption capacity.

Adsorption thermodynamics. With the other conditions constant, the adsorption thermodynamics of lanthanum-iron oxide were evaluated at 298 K, 308 K and 318 K.

RESULTS AND DISCUSSION

Preparation of lanthanum-iron oxide compounds

Lanthanum-iron oxide compounds are synthesized via one-pot solvothermal method using $FeCl_3 \cdot 6H_2O$ and $La(NO_3)_3 \cdot 6H_2O$ as raw materials, and it is used in PMPA removal to evaluate its performance. Fig. 2a displays a histogram representing the adsorption of PMPA by samples with different Fe-to-La molar ratios. The adsorption capacities are 15.61, 31.26, 28.32, 23.98, and 9.96 mg/g for molar ratios of 0:1, 6:1, 8:1, 10:1, and 1:0, respectively. This trend indicates that the adsorption capacity decreases as the proportion of La in the sample diminishes, underscoring the crucial role of La in the adsorption process. Given its superior performance in PMPA adsorption, the sample with a 6:1 Fe-to-La molar ratio is selected for more detailed investigation in subsequent experiments. Fig. 2b demonstrates the adsorption capacities of PMPA onto the lanthanum-iron oxide are 27.93, 28.54, 31.26 and 25.94 mg/g, with the reaction time of 6, 8, 10, 12 h. When the reaction time is less than 10 h, the adsorption capacity gradually decreases, indicating that some of the raw materials have not fully reacted to form lanthanum-iron oxide. The influence of temperature on the adsorption capacity of PMPA over lanthanum-iron oxide is evaluated (Fig. 2c). As can be seen, at temperatures of 200 ℃ and 210 ℃, the adsorption capacities are 31.26 mg/g and 24.05 mg/g, respectively. Besides, high temperature can cause damage to the Teflon-lined stainless steel autoclave. Moreover, the choice of the temperature of 200 ℃ is based on the objective of producing a lanthanum-iron oxide with high adsorbing capacity and minimum waste of energy which is very interesting from an economic point of view. Finally, it is determined that a sample with an iron-lanthanum molar ratio of 6:1, a reaction temperature of 200 ℃, and reaction time of 10 h, has the highest adsorption capacity for PMPA.

Characterization of lanthanum-iron oxide

SEM characterization. The morphology of lanthanum-iron oxide samples with varying Fe-to-La molar ratios have been characterized by SEM in Fig. 3. Fig. 3a demonstrates that at a 6:1 ratio, the sample comprises densely packed, randomly oriented particles, with sizes ranging from 20 to 200 nm. In contrast, at higher ratios of 8:1 (Fig. 3b) and 10:1 (Fig. 3c), the particles exhibit a spherical shape and uniform size distribution with a diameter of approximately 170 nm. This morphological shift is attributed to the reduced molar ratio of $La(NO_3)_3 \cdot 6H_2O$ in the synthesis process, favoring the predominant formation of Fe_3O_4 microspheres in the product.

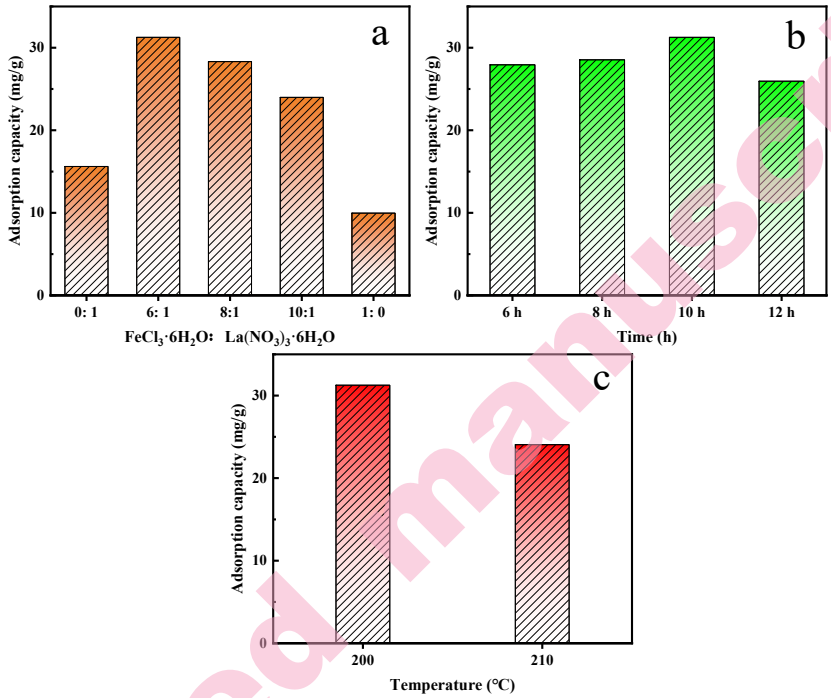

Fig.2. The effect of Fe-to-La molar ratios(a), reaction time(b), and temperature(c) on the removal of PMPA onto lanthanum-iron oxide.

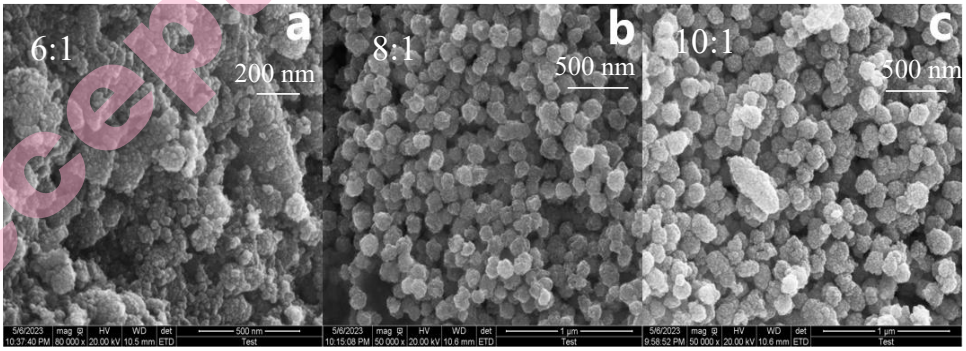

Fig. 3. SEM images of lanthanum-iron oxide compounds with different Fe-to-La molar ratios: (a) 6:1, (b) 8:1, and (c) 10:1.

FTIR measurement. FTIR spectroscopy is utilized to analyze five lanthanum-iron oxide samples with varying Fe-to-La molar ratios, as depicted in Fig. 4a. The peaks at 1600 and 3420 cm^{-1} correspond to the stretching and bending vibrations of O-H bonds on the surface of the material.[30-31] The peak at 1450 cm^{-1} is due to the stretching vibration of the La-bonding hydroxyl groups (La-OH bonds).[32-33] Notably, the peaks at 575 and 636 cm^{-1} are ascribed to Fe-O and La-O bonds,

respectively.[10, 34] A noteworthy trend is observed where the intensity of the La-O bond peak (636 cm^{-1}) gradually diminished with increasing $FeCl_3 \cdot 6H_2O$ dosage. Particularly for ratios of 8:1 and 10:1, the La-O bond peak vanished, whereas the Fe-O bond peak (575 cm^{-1}) became more prominent. At a molar ratio of 6:1, the FTIR spectrum clearly demonstrated the coexistence of both characteristic Fe-O and La-O bond peaks in the sample.

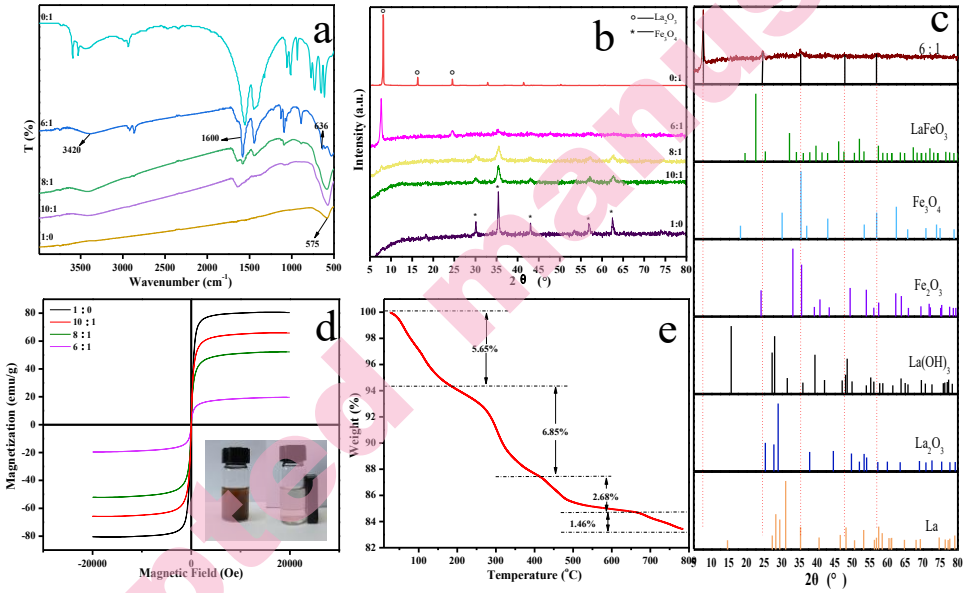

Fig. 4. (a) FTIR spectra of lanthanum-iron oxides with varying Fe-to-La molar ratios: 0:1, 6:1, 10:1, and 1:0. (b) XRD patterns of lanthanum-iron oxides with Fe-to-La molar ratios of 0:1, 6:1, 10:1, and 1:0. (c) Comparison of the XRD patterns of lanthanum-iron oxide with a 6:1 Fe-to-La molar ratio and reference materials. (d) Vibrating sample magnetometry (VSM) analysis of lanthanum-iron oxides with Fe-to-La molar ratios of 6:1, 10:1, and 1:0. (e) Thermogravimetric analysis (TGA) of lanthanum-iron oxide with a 6:1 Fe-to-La molar ratio.

XRD analysis. Fig. 4b presents the XRD patterns of lanthanum-iron oxide compounds with five different Fe-to-La molar ratios. For a molar ratio of 1:0, distinct diffraction peaks were noted at 2θ angles of 30.05°, 35.43°, 43.08°, 56.96°, and 62.45°, indicative of the sample's excellent crystallinity. Moreover, these peaks align precisely with the (220), (311), (400), (511), and (440) crystal planes of standard Fe_3O_4 as per JCPDS card no. 19-0629 in the XRD library.[35] The XRD pattern of the as-synthesized magnetic sample with a molar ratio of 6:1 did not match those of the $LaFeO_3$, Fe_3O_4, Fe_2O_3, $La(OH)_3$, La_2O_3, and La reference materials (Fig. 4c). With an increase in the $La(NO_3)_3 \cdot 6H_2O$ content, leading to a decrease in the Fe-to-La molar ratio from 10:1 to 0:1, new diffraction peaks for lanthanum oxide emerged at 7.68°, 16.39°, and 24.59°, each becoming

progressively more intense. The appearance of the peak at 7.68° indicates the generation of a new phase. The higher the lanthanum ion content, the stronger the peak intensity at 7.68° and the higher the crystallinity. This finding indicates that a new crystal type of lanthanum-iron oxide is obtained through the one-pot method, demonstrating the potential of adjusting the Fe-to-La molar ratio to tailor the material's structural properties.

BET measurements. The specific surface areas and pore characteristics of lanthanum-iron oxides with different molar ratios are summarized in Table 1. For Fe-to-La molar ratios of 6:1, 8:1, and 10:1, large specific surface areas of 73.64, 63.02, and 79.94 m^2/g, respectively, are obtained. These observations indicate that the incorporation of Fe and La metals on the Fe-to-La 1:0 and 0:1 (hydr)oxides are different from that of the other three type. In addition, compared with Fe-to-La 1:0, the introduction of lanthanum increases the specific surface area of the lanthanum-iron oxide, which is conducive to the enrichment of target molecules. [27, 36]

TABLE 1. Physical characteristics of lanthanum-iron oxides with different molar ratios.

$FeCl_3 \cdot 6H_2O$:$La(NO_3)_3 \cdot 6H_2O$	BET surface area (m^2/g)	Total pore volume (cm^3/g)	Average pore diameter (nm)
1:0	26.64	0.0136	1.92
6:1	73.64	0.0395	2.06
8:1	63.02	0.0345	2.01
10:1	79.94	0.0436	2.05
0:1	1.28	0.0009	2.6

VSM measurement. Fig. 4d illustrates the magnetic properties of the lanthanum-iron oxide compounds with varying Fe-to-La molar ratios. Notably, the saturation magnetization values for molar ratios of 1:0, 10:1, 8:1, and 6:1 are 80.5, 65.6, 51.7, and 18.8 emu/g, respectively. All samples exhibit no obvious remanence and coercivity, indicating their superparamagnetic nature. The hysteresis loop diagram highlights that the saturation magnetization decreases as the dosage of $La(NO_3)_3 \cdot 6H_2O$ increases, attributable to the decreasing Fe content in the compounds. Despite this, the sample with a 6:1 molar ratio maintains excellent magnetic responsiveness, as evident in the inset.

TGA analysis. TGA of lanthanum-iron oxide have been presented in Fig. 4e. The decomposition process can be divided into three stages. The initial stage, from RT to 184 ℃, involves a 5.65% weight loss due to the evaporation of surface-adsorbed water. The second stage, spanning 184 to 418 °C, shows a minimal weight loss of 6.85%, mainly due to the minimal decomposition of acetate and nitrate. The final stage, from 418 to 800 °C, entails two phases of weight loss: 2.68% and 1.46%. During this stage, the oxygen-containing groups on the surface of lanthanum-iron oxides were completely eliminated, leaving 83 wt% of lanthanum-iron ash.

XPS analysis. To further investigate the electronic valence of the elements, XPS was utilized to characterize the sample with a 6:1 Fe-to-La molar ratio, as shown in Fig. 5. The full spectrum (Fig. 5a) reveals characteristic peaks for La 3d, Fe 2p, O 1s, and C 1s, confirming the presence of La, Fe, O, and C elements in the synthesized material. The detection of C can be attributed to atmospheric moisture absorption, leading to minor carbonate formation. In Fig. 5b, the La $3d_{3/2}$ and La $3d_{5/2}$ peaks occur at 851.9 and 835.1 eV, respectively,[29] with a binding energy of 16.8 eV, indicative of La in the +3 oxidation state.[37] The Fe 2p spectrum in Fig. 5c exhibits Fe $2p_{1/2}$ and Fe $2p_{3/2}$ peaks at 724.4 and 710.7 eV, respectively, characteristic of both Fe^{2+} and Fe^{3+} states. The O 1s spectrum in Fig. 5d predominantly consists of lattice oxygen, alongside surface-adsorbed oxygen or hydroxyl groups, corresponding to the Fe-O and La-O bonds and oxyhydroxides in the lanthanum-iron oxide compound. These findings offer a comprehensive insight into the structural and chemical properties of lanthanum-iron oxide, particularly in relation to its Fe-to-La ratio-dependent morphology and elemental composition.[38]

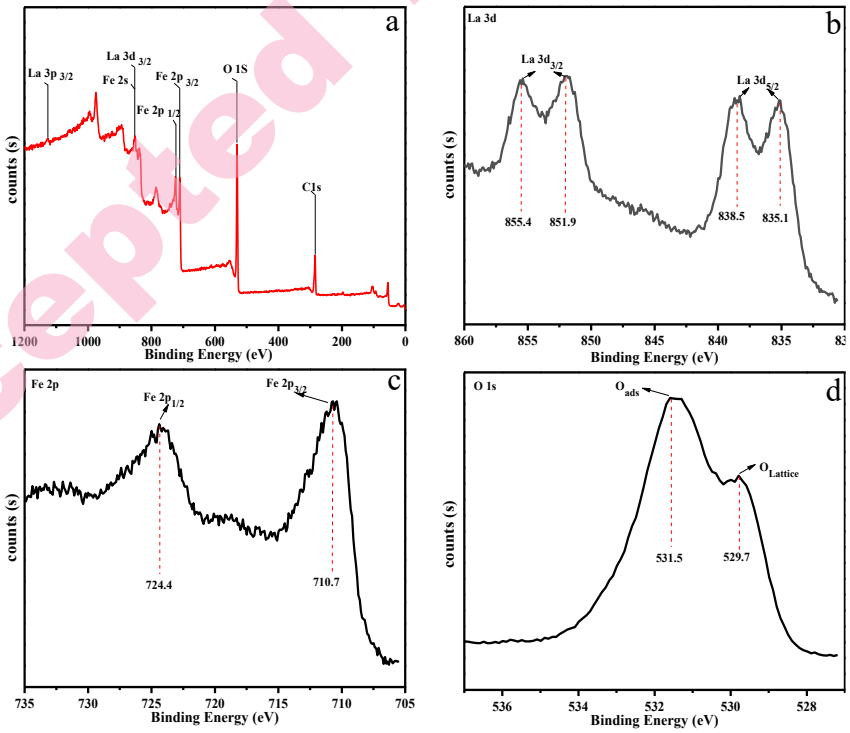

Fig. 5. XPS spectra of lanthanum-iron oxide with a 6:1 Fe-to-La molar ratio. (a) lanthanum-iron oxide, (b) La 3d, (c) Fe 2p, and (d) O 1s spectra.

Adsorption of PMPA

Effect of adsorbent dosage on PMPA adsorption. Fig. 6a demonstrates the relationship between the dosage of lanthanum-iron oxide and its adsorption capacity for PMPA. With increasing dosage, there is a noticeable decrease in PMPA adsorption, while the removal rate significantly improves.[20,39] This observation suggests an increase in available adsorption sites on the lanthanum-iron oxide surface. However, the concentration of PMPA remains constant, this indicates that the adsorption process has not reached saturation. The removal rate of PMPA notably rises from 18.61% to 60.30% as the lanthanum-iron oxide dosage increases, highlighting that a dosage of 35 mg is optimally utilized.

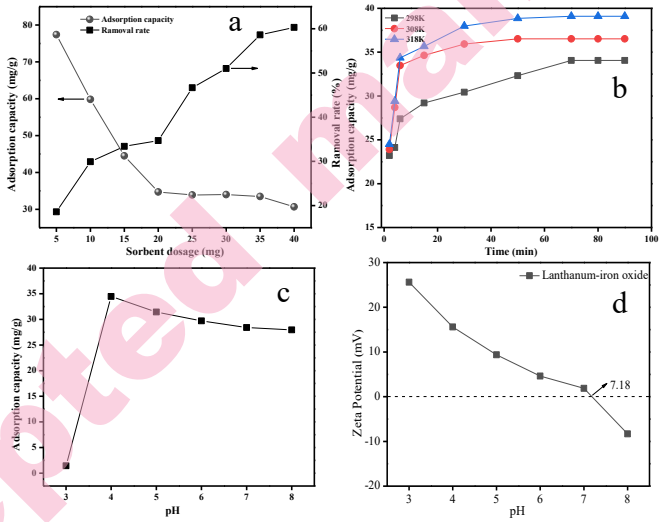

Fig. 6. Influence of adsorbent dosage(a), temperature(b), pH(c) on PMPA adsorption, and zeta potential of lanthanum-iron oxide(d).

Effect of temperature on PMPA adsorption. Concerning the influence of temperature on adsorption, as depicted in Fig. 6b, the process appears to be endothermic. With an increase in temperature from 25 to 45 °C, the maximum adsorption capacity rises from 34.06 to 39.10 mg/g, suggesting that higher temperatures are more conducive to the adsorption process. Consequently, 25 °C was chosen as the experimental temperature based on energy saving considerations.

Effect of pH on PMPA adsorption. Fig. 6c elucidates the impact of pH on PMPA adsorption by lanthanum-iron oxide. The adsorption capacity is enhanced with an increase in pH from 3 to 4, which is primarily attributed to two factors: electrostatic attraction between negatively charged PMPA and positively charged lanthanum-iron oxide (Fig. 6d); Ligand exchange occurs via the -OH in

lanthanum-iron oxide and phosphate group in tenofovir. Moreover, the protonation process that occurs under acidic conditions likely facilitates the ligand exchange process. For instance, $-OH_2^+$ (protonated state) has been reported to be more easily replaced than its original state (-OH).[40] Considering these results, a possible removal mechanism is proposed, as depicted in Fig. S1. Therefore, these effects significantly enhance the adsorption capacity. At pH 4.0, the adsorption reaches a maximum of 34.48 mg/g. Beyond pH 4.0, the removal rate gradually decreases due to competition from hydroxide ions at higher pH levels with negatively charged PMPA.[29, 41] In summary, the primary removal mechanism involves electrostatic attraction and inner-sphere complexation through ligand exchange.

Adsorption kinetics. The adsorption kinetics were analyzed using pseudo-first-order (Eq. (S1)) and pseudo-second-order (Eq. (S2)) reaction kinetic models, providing a deeper understanding of the adsorption mechanisms and kinetics under different experimental conditions. Fig. S2 presents the kinetic analysis of PMPA adsorption on lanthanum-iron oxide. The pseudo-first-order reaction model yielded a correlation coefficient (R^2) of 0.9603 (Fig. S2a), suggesting a lower fit to the experimental data compared to the pseudo-second-order model, which displayed a higher correlation coefficient of 0.9981 (Fig. S2b). Furthermore, Table 2 compares the experimentally obtained equilibrium adsorption capacity ($q_{e,exp}$) with the calculated values ($q_{e,cal}$) from the pseudo-second-order model, showing a close agreement. This finding indicates that the adsorption capacity is directly related to the number of active sites on the lanthanum-iron oxide surface and suggests that chemical adsorption might be the rate-limiting step in this process.

TABLE 2. Kinetic parameters for PMPA adsorption on lanthanum-iron oxide.

C_0 (mg/L)	$q_{e,exp}$ (mg/g)	Pseudo-first-order			Pseudo-second-order		
		k_1	$q_{e,cal}$ (mg/g)	R^2	k_2	$q_{e,cal}$ (mg/g)	R^2
50	33.92	2.57×10^{-2}	16.38	0.9603	8.85×10^{-3}	35.01	0.9981

Isothermal adsorption study. The study further involved fitting the adsorption data to the Langmuir (Eq. (S3)) and Freundlich (Eq. (S4)) isothermal adsorption models. Fig. S3 illustrates the adsorption isotherm plots of PMPA at various initial concentrations at RT, the correlation coefficients, R_L^2 and R_F^2, for these models are 0.9937 and 0.5461, respectively. The higher R_L^2 value compared to R_F^2 suggests that the Langmuir model, which assumes monolayer adsorption, is a better fit for describing the adsorption behavior of PMPA on lanthanum-iron oxide. According to Table 3, the maximum adsorption capacity of lanthanum-iron oxide for PMPA, as determined by the Langmuir model, is 37.36 mg/g. This value closely aligns with the experimentally calculated maximum adsorption of 34.06 mg/g, further supporting the applicability of the Langmuir model in this context.

TABLE 3. Freundlich and Langmuir isotherm parameters for the adsorption of PMPA on lanthanum-iron oxide.

Temperature (K)	$q_{e,exp}$ (mg/g)	Langmuir				Freundlich	
		q_{max} (mg/g)	k_L (L/mg)	R^2	n	k_F (mg/g)	R^2
298	34.06	37.36	0.49	0.9937	15.33	28.11	0.5461

Adsorption thermodynamics. The thermodynamic parametric equations are shown in Eqs. (Eq(S5), Eq(S6)). As can be seen in Fig. S4, the ΔH^0 and ΔS^0 parameters for PMPA are calculated from the slope and intercepts of a lnKc vs 1/T graph. The related thermodynamic values are shown in Table 4, both ΔH^0 and ΔS^0 are greater than zero, indicating that the process is an entropy-increasing and heat absorption process. The preferential polar interactions, which are associated with the release of water molecules between the hydration layers of the adsorbent and adsorbate. All the values of ΔG^0 are negative at different temperatures and the Gibbs free energy decrease with the temperature increasing, indicating that PMPA adsorption on lanthanum-iron oxide proceeds spontaneously.

TABLE 4. Thermodynamic parameters for the adsorption of PMPA on lanthanum-iron oxide.

		ΔG (kJ·mol^{-1})		
		298K	308K	318K
0.0120	43.14	-12.85	-13.28	-13.78

A comparison of lanthanum-iron oxide with other adsorbents, including magnetic, non-magnetic and bimetal materials, which widely used for the treatment of pharmaceutical wastewater,[20, 29, 42, 43] and the relevant data are summarized in Table S1. Clearly, it is easy for lanthanum-iron oxide to separate from the solution by an external magnetic field, which is conducive to the separation and recovery of adsorbents. In addition, lanthanum-iron oxide is easy to prepare and exhibits high adsorption capacity.

CONCLUSION

In this study, we successfully synthesized lanthanum-iron oxide compounds using a streamlined one-pot method, employing EG as the solvent and $FeCl_3 \cdot 6H_2O$ and $La(NO_3)_3 \cdot 6H_2O$ as the primary materials. This approach, in contrast to traditional methods such as high-energy milling, citrate-gel method, and co-precipitation, eliminates the need for step-by-step sample processing. Moreover, it offers significant advantages over the microwave-assisted one-step method by obviating the need for pH adjustment, thus enhancing efficiency and energy savings. SEM analysis revealed that the lanthanum-iron oxide compound comprises densely packed particles with sizes ranging from 20 to 200 nm. FTIR validated the existence of Fe-O (575 cm^{-1}) and La-O (636 cm^{-1}) bonds, while XRD

analysis showed that a new crystal type of lanthanum iron oxide was produced by the employed one-pot method. VSM highlighted the superparamagnetic nature of the samples, which enables rapid separation under an external magnetic field. XPS results confirmed the co-presence of La, Fe, O, and C elements in the sample. The synthesized lanthanum-iron oxide was then employed in the study of tenofovir ((*R*)-9-(2-phosphonomethoxypropyl)adenine, PMPA) adsorption. The kinetic and isothermal adsorption models suggested that the adsorption behavior is best described by the pseudo-second-order kinetic model and the Langmuir isothermal model, indicative of a monolayer chemical adsorption mechanism. Meanwhile, the spontaneous and endothermic process is indicated by adsorption thermodynamics. The mechanism of PMPA adsorption on lanthanum-iron oxide was identified as inner-sphere complexation and electrostatic attraction. This study not only presents an innovative method for synthesizing lanthanum-iron oxide materials but also demonstrates their potential as adsorbents for the treatment of actual phosphate-containing wastewater.

SUPPLEMENTARY MATERIAL

Additional data are available electronically at the pages of journal website: https://www.shd-pub.org.rs/index.php/JSCS/article/view/13599, or from the corresponding author on request.

Author disclosure statement: The authors report that there are no competing interests to declare.

Acknowledgments: The authors acknowledge the assistance of the JLICT Center of Characterization and Analysis. This work was supported by the Jilin Provincial Department of Science and Technology under grant numbers 20230203164SF and the Natural Science Foundation of China under grant number 22106051.

И З В О Д

ЕФИКАСНА СОЛВОТЕРМАЛНА СИНТЕЗА ЛАНТАН-ГВОЖЂЕ-ОКСИДА У ЈЕДНОМ КОРАКУ И ПРИМЕНА У АДСОРПЦИЈИ ТЕНОФОВИРА

ZHIGANG LIU[1], PING XU[2], SHIHUA YU[2], XIANG LI[1], XIAODAN ZENG[3], JIBO ZHANG[1], AND JUNJING HAO[4]

[1]College of Petrochemical Technology, Jilin University of Chemical Technology, Jilin 132022, China, [2]College of Chemical & Pharmaceutical Engineering, Jilin University of Chemical Technology, Jilin 132022, China, [3]Centre of Analysis and Measurement, Jilin Institute of Chemical Technology, Jilin 132022, China, and [4]China Petroleum Jilin Chemical Engineering Co., Ltd., Jilin 132000, China.

Нови магнетни композити лантан-гвожђе-оксида синтетизовани су коришћењем методе у једном кораку. Предложени приступ поједностављује процес синтезе захваљујући избегавању традиционалних захтева као што су подешавање pH вредности и калцинација на високим температурама, што резултира ефикаснијим поступком и производњом магнетног материјала. Испитан је утицај односа Fe-La, времена реакције и температуре реакције на својства и адсорпционе перформансе композита лантан-гвожђе-оксида. Синтетизовани композити су окарактерисани методама SEM, XRD, VSM, FTIR, BET, TGA и XPS, чиме је утврђено да се узорци састоје од насумично оријентисаних честица величина од 20 до 200

nm, да поседују одличну кристалиничност, магнетну осетљивост и термичку стабилност. Поред тога, у овом истраживању синтетисани лантан-гвожђе-оксиди су примењени за адсорбовање тенофовира ((*R*)-9-(2-фосфонометоксипропил)аденина, PMPA), са максималним капацитетом адсорпције од 34,06 mg/g, при дози адсорбента = 0,9 g/L, pH = 4, *C* = 50 mg/L и *T* = 25 °C. Ово истраживање је показало да је примењена метода једноставна за припрему лантан-гвожђе-оксида, који се лако одваја од третиране воде, што је корисно за практичну примену.

(Примљено 25. октобра 2025; ревидирано 26. јануара 2026; прихваћено 1. јула 2026.)

REFERENCES

1. G. Shabbir, A. H. Qureshi, K. Saeed, *Mater. Lett.* **60** (2006) 3706 (https://doi.org/10.1016/j.matlet.2006.03.093)
2. A. Kasick, A. A. Hajer, K. D. Wolfe, S. Velraj, D. A. Daramola, J. P. Trembly, *J. Electrochem. Soc.* **170** (2023) 104509 (https://doi.org/10.1149/1945-7111/acff19)
3. M. Pudukudy, Z. Yaakob, Q. Jia, M. S. Takriff, *Appl. Surf. Sci.* **467** (2019) 236 (https://doi.org/10.1016/j.apsusc.2018.10.122)
4. H. Shen, T. Xue, Y. Wang, G. Cao, Y. Lu, G. Fang, *Mater. Res. Bull.* **84** (2016) 15 (https://doi.org/10.1016/j.materresbull.2016.07.024)
5. I. N. Sora, F. Fontana, R. Passalacqua, C. Ampelli, S. Perathoner, G. Centi, F. Parrino, L. Palmisano, *Electrochim. Acta* **109** (2013) 710 (v https://doi.org/10.1016/j.electacta.2013.07.132)
6. K. K. Bhargav, S. Ram, S. B. Majumder, *J. Appl. Phys.* **115** (2014) 204109 (https://doi.org/10.1063/1.4879899)
7. J. Yang, H. Zhang, K. Tian, Y. Zhang, J. Zhang, *J. Environ. Manage.* **340** (2023) 117975 (https://doi.org/10.1016/j.jenvman.2023.117975)
8. M. Ismael, M. Wark, *Catalysts* **9** (2019) 342 (https://doi.org/10.3390/catal9040342)
9. J. Yang, H. Zhong, M. Li, L. Zhang, Y. Zhang, *React. Kinet. Catal. Lett.* **97** (2009) 269 (https://doi.org/10.1007/s11144-009-0025-1)
10. N. T. Thuy, D. L. Minh, *Adv. Mater. Sci. Eng.* **2012** (2012) 380306 (https://doi.org/10.1155/2012/380306)
11. T. A. Nguyen, V. N. T. Pham, H. T. Le, D. H. Chau, I. Y. Mittova, *Ceram. Int.* **45** (2019) 21768 (https://doi.org/10.1016/j.ceramint.2019.07.178)
12. S. Thirumalairajan, K. Girija, I. Ganesh, D. Mangalaraj, C. Viswanathan, A. Balamurugan, N. Ponpandian, *Chem. Eng. J.* **209** (2012) 420 (https://doi.org/10.1016/j.cej.2012.08.012)
13. S. Thirumalairajan, K. Girija, N. Y. Hebalkar, D. Mangalaraj, C. Viswanathan, N. Ponpandian, *RSC Adv.* **3** (2013) 7549 (https://doi.org/10.1039/C3RA00006K)
14. M. Khorasani-Motlagh, M. Noroozifar, A. Ahanin-Jan, *J. Iran. Chem. Soc.* **9** (2012) 833 (https://doi.org/10.1007/s13738-012-0100-9)
15. P. Wang, J. Yan, S. Wang, P. Xu, L. Shen, T. Song, *Bioresour. Technol.* **340** (2021) 125641 (https://doi.org/10.1016/j.biortech.2021.125641)
16. M. E. Barkil, M. C. Gagnieu, J. R. M. Guitton, *J. Chromatogr. B* **854** (2007) 192 (https://doi.org/10.1016/j.jchromb.2007.04.015)
17. M. Yang, J. Shi, Z. Xu, S. Zhu, Y. Cui, *J. Environ. Manage.* **231** (2019) 207 (https://doi.org/10.1016/j.jenvman.2018.10.036)

18. A. J. Toth, E. Haaz, B. Szilagyi, T. Nagy, A. J. Tarjani, D. Fozer, A. Andre, N. Valentinyi, S. Solti, P. Mizsey, *Waste Treat. Recov.* **3** (2018) 1 (https://doi.org/10.1515/wtr-2018-0001)
19. C. Mansas, L. Atfane-Karfane, E. Petit, J. Mendret, S. Brosillon, A. Ayral, *J. Environ. Chem. Eng.* **8** (2020) 104043 (https://doi.org/10.1016/j.jece.2020.104043)
20. J. R. Li, H. Wang, X. Wang, J. Ye, X. Wang, B. Xue, *Mater. Chem. Phys.* **343** (2025) 131005 (https://doi.org/10.1016/j.matchemphys.2025.131005)
21. E. S. Muzawazi, N. Thusabantu, A. E. Oluwalana-Sanusi, N. Mukaratirwa-Muchanyereyi, G. Mamba, P. Mokoena, N. Mabuba, N. Chaukura, *Int. J. Environ. Sci. Technol.* **4** (2024) 21 (https://doi.org/10.1007/s13762-023-05201-3)
22. R. J. Fickelscherer, C. M. Ferger, S. A. Morrissey, *AIChE J.* **67** (2021) 17169 (https://doi.org/10.1002/aic.17169)
23. S. W. Zou, K. Y. Koh, Z. H. Chen, Y. Y. Wang, J. P. Chen, Y. M. Zheng, *Chemosphere* **288** (2022) 132634 (https://doi.org/10.1016/j.chemosphere.2021.132634)
24. R. Xu, M. Zhang, R. J. Mortimer, G. Pan, *Environ. Sci. Technol.* **51** (2017) 3418 (https://doi.org/10.1021/acs.est.6b05623)
25. X. Wang, Y. Li, X. Wen, L. Liu, L. Zhang, M. Long, *Water Res.* **249** (2024) 120969 (https://doi.org/10.1016/j.watres.2023.120969)
26. L. Tang, W. Chen, F. Li, J. Xu, Y. Shi, H. Jiang, *Chem. Eng. J.* **482** (2024) 148410 (https://doi.org/10.1016/j.cej.2023.148410)
27. H. Duan, L. Zhang, Y. Wang, Y. Liu, Y. Wang, *Environ. Sci. Pollut. Res.* **28** (2021) 626620 (https://doi.org/10.1007/s11356-021-15127-3)
28. H. X. Xiong, S. N. Peng, D. Zhang, *Mater. Chem. Phys.* **285** (2022) 126195 (https://doi.org/10.1016/j.matchemphys.2022.126195)
29. S. Ajebli, G. Kaichouh, M. Khachani, H. Babas, M. El Karbane, I. Warad, Z. S. Safi, A. Berisha, V. Mehmeti, A. Guenbour, A. Bellaouchou, A. Zarrouk, *Chem. Phys. Lett.* **801** (2022) 139676 (https://doi.org/10.1016/j.cplett.2022.139676)
30. F. E. García, M. I. Litter, I. N. Sora, *ChemistryOpen* **10** (2021) 790 (https://doi.org/10.1002/open.202100065)
31. Q. Song, S. Huang, L. Xu, N. Wang, Z. Hu, X. Luo, Z. Zheng, *Sci. Total Environ.* **723** (2020) 137838 (https://doi.org/10.1016/j.scitotenv.2020.137838)
32. C. Y. Liu, Y. L. Wang, X. L. Li, J. Y. Li, S. X. Dong, H. T. Hao, Y. Tong, Y. Q. Zhou, *J. Environ. Sci.* **120** (2022) 18 (https://doi.org/10.1016/j.jes.2022.01.003)
33. Y. Wang, C. Guo, Y. Liu, X. Li, Y. Liu, R. Naidu, M. M. Rahman, *J. Water Process Eng.* **71** (2025) 107347 (https://doi.org/10.1016/j.jwpe.2025.107347)
34. K. M. S. Khalil, A. H. Mahmoud, M. Khairy, *Adv. Powder Technol.* **33** (2022) 103429 (https://doi.org/10.1016/j.apt.2022.103429)
35. P. Yang, B. Zhu, J. Zhao, H. Yu, L. Yan, Q. Wei, B. Du, *Inorg. Chim. Acta* **408** (2013) 120 (https://doi.org/10.1016/j.ica.2013.09.010)
36. H. Zhang, W. Tong, H. Li, C. Li, M. Ma, Z. Dong, G. Zhang, J. Qu, Y. Zhang, *J. Cleaner Prod.* **490** (2025) 144620 (https://doi.org/10.1016/j.jclepro.2024.144620)
37. C. Li, D. Ma, S. Mou, Y. Luo, B. Ma, S. Lu, G. Cui, Q. Li, Q. Liu, X. Sun, *J. Energy Chem.* **50** (2020) 402 (https://doi.org/10.1016/j.jechem.2020.03.044)
38. M. I. Díez-García, R. Gomez, *ChemSusChem* **10** (2017) 2457 (https://doi.org/10.1002/cssc.201700166)
39. Z. Li, Y. Wei, H. Wu, P. Yuan, H. Bu, X. Tan, *Sep. Purif. Technol.* **360** (2025) 130642 (https://doi.org/10.1016/j.seppur.2024.130642)

40. B. Wang, H. Zhang, X. Hu, R. Chen, W. Guo, H. Wang, C. Wang, J. Yuan, J. Chen, S. Xia, *Chemosphere* **312** (2023) 137149 (https://doi.org/10.1016/j.chemosphere.2022.137149)
41. Y. Lu, X. Jin, X. Li, M. Liu, B. Liu, X. Zeng, J. Chen, Z. Liu, S. Yu, Y. Xu, *Polymers* **15** (2023) 15010248 (https://doi.org/10.3390/polym15010248)
42. P. Yadav, A. Yadav, P. K. Labhasetwar, *Environ. Sci. Pollut. Res.* **29** (2022) 37204 (https://doi.org/10.1007/s11356-021-18385-3)
43. R. Mudhulkar, K. Damarla, V. N. Pappula, *Anal. Methods* **14** (2022) 449 (https://doi.org/10.1039/d1ay01772a).